Inorganic Chemistry
Article

Inorg. Chem. **2010**, *49*, 1133–1143 **1133**
DOI: 10.1021/ic902069w

Magnetic Ordering in Nitrides with the η-Carbide Structure, $(Ni,Co,Fe)_2(Ga,Ge)Mo_3N$

Lev A. Sviridov,[†] Peter D. Battle,*[,†] Fernande Grandjean,[‡] Gary J. Long,[§] and Timothy J. Prior[∥]

[†]*Inorganic Chemistry Laboratory, University of Oxford, South Parks Road, Oxford, OX1 3QR, United Kingdom,* [‡]*Department of Physics, University of Liège, B5, B-4000 Sart-Tilman, Belgium,* [§]*Department of Chemistry, Missouri University of Science and Technology, University of Missouri, Rolla, Missouri 65409-0010, and* [∥]*Department of Chemistry, University of Hull, Cottingham Road, Kingston upon Hull, HU6 7RX, United Kingdom*

Received October 20, 2009

Compositions in the series $Ni_{2-x}Co_xGeMo_3N$ ($0 \le x \le 2$), $Co_2Ge_{1-x}Ga_xMo_3N$ ($0 < x \le 0.7$), $Co_{2-x}Fe_xGeMo_3N$ ($0 \le x \le 2$), and $Co_{2-x}Fe_xGe_{0.5}Ga_{0.5}Mo_3N$ ($0 \le x \le 0.8$) have been synthesized by the reductive nitridation of binary oxides and studied by appropriate combinations of magnetometry, transport measurements, neutron diffraction, and Mössbauer spectroscopy. All of these compositions adopt the cubic η-carbide structure ($a \sim 11.11$ Å) and show a resistivity of $\sim 10^{-3}$ Ω cm. No long-range magnetic order was observed in $Ni_{2-x}Co_xGeMo_3N$, although evidence of spin freezing was observed in Co_2GeMo_3N. The introduction of gallium into this composition leads to the onset of antiferromagnetic ordering at 90 K in $Co_2Ge_{0.3}Ga_{0.7}Mo_3N$. The magnetic structure consists of an antiferromagnetic arrangement of ferromagnetic Co_4 groups, with an ordered magnetic moment of 0.48(9) μ_B per cobalt atom. The same magnetic structure is found in $Co_{0.5}Fe_{1.5}GeMo_3N$ and $Co_{1.2}Fe_{0.8}Ge_{0.5}Ga_{0.5}Mo_3N$. The former orders above room temperature with an average moment of 1.08(3) μ_B per transition-metal site, and the latter at 228 K with an average moment of 1.17(4) μ_B per site. The magnetic behavior of these compounds is discussed in terms of the electron count within each series.

Introduction

The cubic interstitial carbide Fe_3Mo_3C was the first compound to be described as an η-carbide phase.[1] The interest in this material and related compositions originally stemmed from their hardness, although recent attention has focused on their potential as catalysts.[2] Many nitrides, for example, Fe_3Mo_3N, belong to the same structural family and also show significant catalytic activity.[3−5] They have usually been synthesized via a mixed-metal oxide, which is then nitrided by reaction with ammonia. $FeMoO_4$, for example, can be prepared as a precursor and subsequently converted to Fe_3Mo_3N.[6,7] The success of the synthesis depends in part on the relative stability of the target structure and its competitors. This in turn depends on the particular chemical elements that are present. For example, attempts to prepare Ni_3Mo_3N have resulted in the formation of Ni_2Mo_3N,[8−10] which adopts the filled β-Mn structure. In contrast, Fe_3Mo_3N forms more readily than Fe_2Mo_3N; the latter has never been fully characterized.[11] The available evidence suggests that electron-rich metals from group 10 of the periodic table stabilize the β-Mn structure. Indeed, the use of an alternative synthesis route, in which a mixture of binary oxides was heated under a flow of 10% dihydrogen in dinitrogen gas, resulted in the formation of complex β-Mn phases in which a relatively high concentration of iron could be stabilized by the presence of a group 10 metal. Many of the resulting compositions, all of which are metallic, showed ferromagnetic ordering below relatively high Curie temperatures (T_c), for example, T_c = 225 K in the case of $Fe_{1.25}Pt_{0.75}Mo_3N$, with a saturation magnetization (M_{sat}) of 2.10(2) μ_B per formula unit.[12−15]

*To whom correspondence should be addressed. Fax: +44 1865 272690. E-mail: Peter.Battle@chem.ox.ac.uk.

(1) Westgren, A.; Phragmen, G. *Trans. Amer. Soc. Steel Treat.* **1928**, *13*, 539.
(2) Korlann, S.; Diaz, B.; Bussell, M. E. *Chem. Mater.* **2002**, *14*, 4049.
(3) Jacobsen, C. J. H. *Chem. Commun.* **2000**, 1057.
(4) Mckay, D.; Gregory, D. H.; Hargreaves, J. S. J.; Hunter, S. M.; Sun, X. *Chem. Commun.* **2007**, 3051.
(5) Hargreaves, J. S. J. *J. Molecular Catalysis A: Chemical* **2009**, *305*, 125.
(6) Jackson, S. K.; Layland, R. C.; zur Loye, H.-C. *J. Alloys Compd.* **1999**, *291*, 94.
(7) Bem, D. S.; Gibson, C. P.; zur Loye, H.-C. *Chem. Mater.* **1993**, *5*, 397.
(8) Weil, K. S.; Kumta, P. N.; Grins, J. *J. Solid State Chem.* **1999**, *146*, 22.
(9) Jack, K. H. *Metal Powder Report* **1987**, *42*, 478.
(10) Herle, P. S.; Hegde, M. S.; Sooryanarayana, K.; Row, T. N. G.; Subbanna, G. N. *Inorg. Chem.* **1998**, *37*, 4128.
(11) Evans, D. A.; Jack, K. H. *Acta Crystallogr.* **1957**, *10*, 769.
(12) Oldham, S. E.; Battle, P. D.; Blundell, S. J.; Brooks, M. L.; Pratt, F. L.; Prior, T. J. *J. Mater. Chem.* **2005**, *15*, 3402.
(13) Prior, T. J.; Battle, P. D. *J. Solid State Chem.* **2003**, *172*, 138.
(14) Prior, T. J.; Nguyen-Manh, D.; Couper, V. J.; Battle, P. D. *Journal of Physics: Condensed Matter* **2004**, *16*, 2273.

Published on Web 12/23/2009

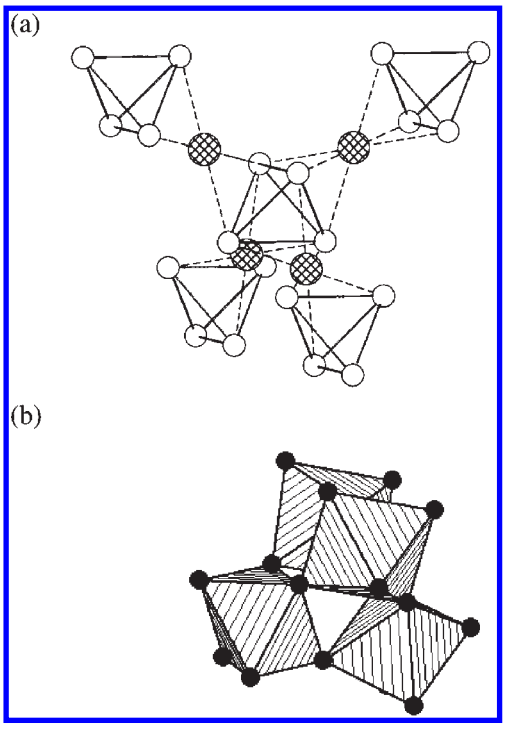

Figure 1. Structural subunits in the η-carbide structure. (a) Atoms on 32*e* sites (white circles) form tetrahedra which are face-capped by atoms on 16*d* sites (hatched circles) to form supertetrahedra; the latter are linked by shared vertices. (b) Mo_6N octahedra share vertices to form tetrahedral units.

However, T_c and M_{sat} were found to be very sensitive to the chemical composition.

In contrast to the β-manganese phases, the η-carbide phases studied to date have shown neither ferromagnetic nor antiferromagnetic ordering. Fe_3Mo_3N and Co_3Mo_3N are metallic, but their magnetic behavior is complex.[6,16] The susceptibilities do not obey the Curie law, nor are they consistent with Pauli paramagnetism. The marked increase in magnetization that occurs on cooling compositions in the solid solution $Fe_{3-x}Co_xMo_3N$ below 30 K was interpreted[17] in terms of superparamagnetic-cluster formation, suggesting the presence of strong interatomic interactions. Neutron diffraction experiments failed to provide any convincing evidence of long-range magnetic ordering.

The crystal chemistry is probably responsible for some aspects of the complex behavior. The chemical formula M_3Mo_3N is more informatively written as $M_2^{32e}M'^{16d}Mo_3N$ to indicate that the first-row transition metals are distributed over two inequivalent sites in the space group $Fd\bar{3}m$. In any study where two such elements are present, allowance must be made for the possibility of atomic ordering over the two sites; in the case of $Fe_{3-x}Co_xMo_3N$, the iron atoms were shown to occupy preferentially the 16*d* sites. The arrangement of the two types of site is illustrated in Figure 1. The atoms on 32*e* sites form tetrahedra which are capped over each face by those occupying 16*d* sites to form supertetrahedra or *stellae quadrangulae*; the supertetrahedra share vertices to form an infinite diamondoid net. Groups of four Mo_6N octahedra share vertices to form tetrahedral clusters which are vertex-linked to give a second diamondoid net. The two nets interpenetrate, the empty space within one being filled by the polyhedra of the other. The high concentration of Fe_4 tetrahedra in Fe_3Mo_3N is likely to result in the frustration of any antiferromagnetic coupling that is present, thus reducing the likelihood of a magnetic ground state being adopted.

The aim of the present study was to synthesize new η-carbide compositions in order to investigate the extent to which the magnetic properties were sensitive to the chemistry of the system. We were encouraged by the observation of both chemically sensitive, high T_c values in β-Mn phases and the enhanced low-temperature magnetization of $Fe_{3-x}Co_xMo_3N$. Our intention was to manipulate the composition, and hence the electron concentration and interatomic distances, in order to induce long-range magnetic ordering in η-carbide compositions. Our initial strategy was to simplify the problem by placing a nonmagnetic element on the 16*d* sites, thus reducing the level of frustration in the infinite net by creating magnetically isolated M_4 (M = Fe, Co, Ni) tetrahedra. We took as our starting point the composition Ni_2GaMo_3N, which has previously been shown[17] to have an ordered distribution of nickel and gallium over the 32*e* and 16*d* sites, respectively. This compound is a weak Pauli paramagnet with a resistivity of 1.2(1) mΩ cm at 290 K. We have now extended our study of compositions in which the 16*d* site is occupied by a p-block element, and we describe below the synthesis and characterization of new compositions in the system (Fe, Co, Ni)$_2$(Ga, Ge)Mo_3N, many of which adopt magnetically ordered ground states.

Experimental Section

Polycrystalline samples of target compositions were synthesized by firing intimately ground, stoichiometric mixtures of iron(III) oxide, cobalt(II,III) oxide, nickel(II) oxide, germanium(IV) oxide, and hydrated gallium(III) nitrate in an alumina crucible under a flow of 10% dihydrogen in dinitrogen; the reactions were unsuccessful when gallium(III) oxide was used as a source of gallium. The mixtures were initially fired as loose powders at 973 K and then pressed into pellets for subsequent firings at temperatures of up to 1248 K. The reaction product was always cooled to room temperature under the gas flow. The progress of the reactions was monitored by X-ray powder diffraction. Data suitable for use in Rietveld analysis[18] were collected with a step size $\Delta 2\theta = 0.0084°$ over the angular range $5 \leq 2\theta/\text{deg} \leq 125$ on a Philips X'Pert PRO diffractometer using Cu Kα_1 radiation. The data were analyzed using the GSAS program suite.[19] The magnetic properties of selected samples were studied using a Quantum Design MPMS 5000 SQUID magnetometer. The sample magnetization was measured in a field of 100 Oe over the temperature range $2 \leq T/\text{K} \leq 350$ after cooling the sample from room temperature to 2 K in both zero applied field (ZFC) and 100 Oe (FC). When appropriate, the sample magnetization was measured at a constant temperature over the field range $-50 \leq H/\text{kOe} \leq 50$; the sample was cooled to the measuring field in a field of 50 kOe.

Electrical resistivity measurements were carried out over the temperature range $80 \leq T/\text{K} \leq 300$ using a four-probe dc technique; data were collected on warming. The samples were in the form of rectangular blocks, approximately 10 × 4 × 2 mm in size, which had been cut from sintered pellets of the

(15) Prior, T. J.; Oldham, S. E.; Couper, V. J.; Battle, P. D. *Chem. Mater.* **2005**, *17*, 1867.
(16) Panda, R. N.; Gajbhiye, N. S. *J. Alloys Compd.* **1997**, *256*, 102.
(17) Prior, T. J.; Battle, P. D. *J. Mater. Chem.* **2004**, *14*, 3001.
(18) Rietveld, H. M. *J. Appl. Crystallogr.* **1969**, *2*, 65.
(19) Larson, A. C.; von Dreele, R. B. *General Structure Analysis System (GSAS)*; LAUR 86−748; Los Alamos National Laboratories: 1994.

reaction product. Copper wires were attached to the block using a silver-loaded epoxy adhesive resin. Each measurement was carried out using a constant current, selected to lie in the range $10 \leq I/\text{mA} \leq 90$. Duplicate measurements on blocks cut from different pellets showed the same qualitative temperature dependence, but the magnitude of the resistivity varied by approximately 25%. Our ability to offer a quantitative interpretation of the resistivity data given below is limited by this variability, which presumably stems from grain-boundary effects in the sintered blocks.

The most interesting samples were studied by neutron diffraction using the powder diffractometer D2b at ILL, Grenoble; the instrument was configured to give a high flux and medium angular resolution. Data were typically collected using a wavelength of ~1.59 Å, if the principal purpose of the experiment was to study the crystal structure, or ~2.4 Å, if the principal purpose was to search for magnetic scattering; unit-cell parameters determined from X-ray data were used to determine more accurate values for the neutron wavelength in each case. The sample, typically of mass ~1.5 g, was contained in a vanadium can of diameter 5 mm. The can was mounted in a Displex refrigerator when data were to be collected below room temperature. The data were analyzed using the GSAS program suite. The peak shape was modeled using a pseudo-Voigt function and the background level by a 12-term Chebyshev polynomial.

The Mössbauer spectrum of a selected sample was measured at 10 and 295 K in a Janis Supervaritemp cryostat with a constant-acceleration spectrometer which utilized a rhodium matrix cobalt-57 source and was calibrated at 295 K with α-iron powder. The Mössbauer spectral absorber contained 40 mg/cm^2 of powder mixed with boron nitride. The statistical errors associated with the isomer shifts, quadrupole shifts, and line widths are tabulated below; the absolute errors of these parameters are approximately twice the statistical errors.

Results

i. $Ni_{2-x}Co_xGeMo_3N$. Our initial strategy was to attempt to substitute cobalt for nickel in Ni_2GaMo_3N. This approach usually resulted in the formation of an η-carbide phase contaminated by a β-manganese impurity, and it was therefore not pursued. However, when gallium was replaced by germanium, we were able to replace nickel with cobalt in a stepwise manner. The X-ray diffraction patterns of samples across the whole composition range were consistent with the presence of only a highly crystalline η-carbide phase. The unit-cell parameter showed a near-linear variation with composition $x = 0$, $a = 11.08745(4)$ Å; $x = 2.0$, $a = 11.0993(2)$ Å. The resistivity of each sample was ~1 mΩ cm and almost constant over the measured temperature range; ρ(T) is shown in Figure 2 for a number of compositions in the $Ni_{2-x}Co_xGeMo_3N$ system. Figure 3 illustrates the typical temperature dependence of the magnetic susceptibility of compositions having $x < 2$. The temperature dependence shown in Figure 3 cannot be modeled using a Curie–Weiss law, nor is it consistent with simple Pauli paramagnetism; the increase in susceptibility observed at low temperature becomes more marked as the cobalt content increases. It appears that localized and itinerant electrons coexist in these compositions. Figure 4a illustrates the temperature dependence of the magnetic susceptibility of Co_2GeMo_3N. Both the ZFC and FC susceptibilities suggest that a magnetic phase transition occurs at 8 K. Unfortunately, hysteresis, probably attributable to the presence of a low concentration of ferromagnetic cobalt metal, is apparent over the whole of the measured temperature range, and it is not clear whether the susceptibility maximum represents a transition to an antiferromagnetic state or to a more complex magnetic state, for example, a spin-glass state. The variation of M(H) at 300 K, shown in Figure 4b, supports the supposition that

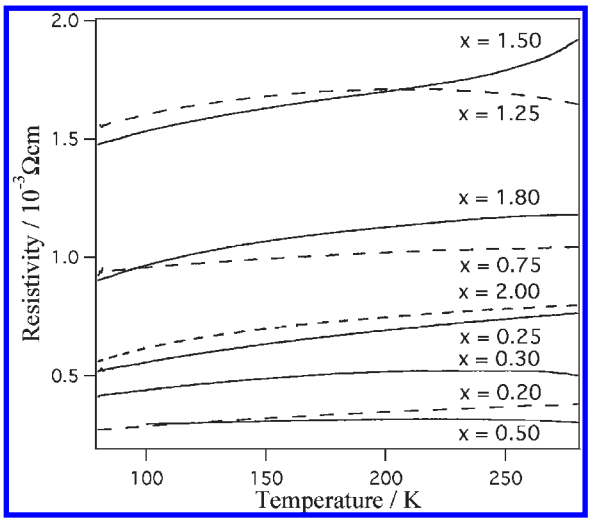

Figure 2. Temperature dependence of the resistivity of $Ni_{2-x}Co_xGeMo_3N$.

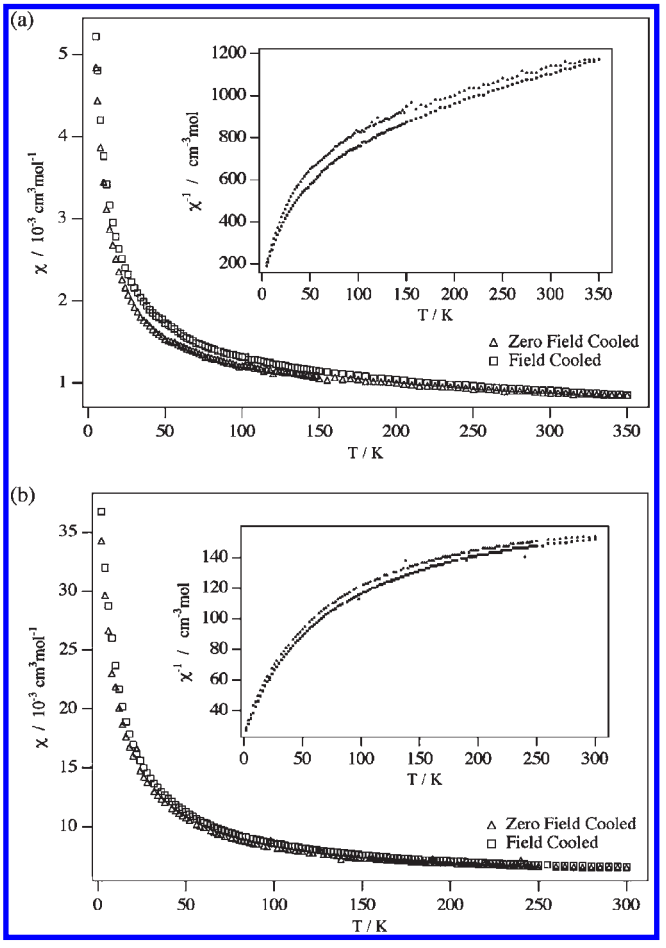

Figure 3. Temperature dependence of the molar magnetic susceptibility of $Ni_{2-x}Co_xGeMo_3N$ for (a) $x = 0.4$ and (b) $x = 1.7$.

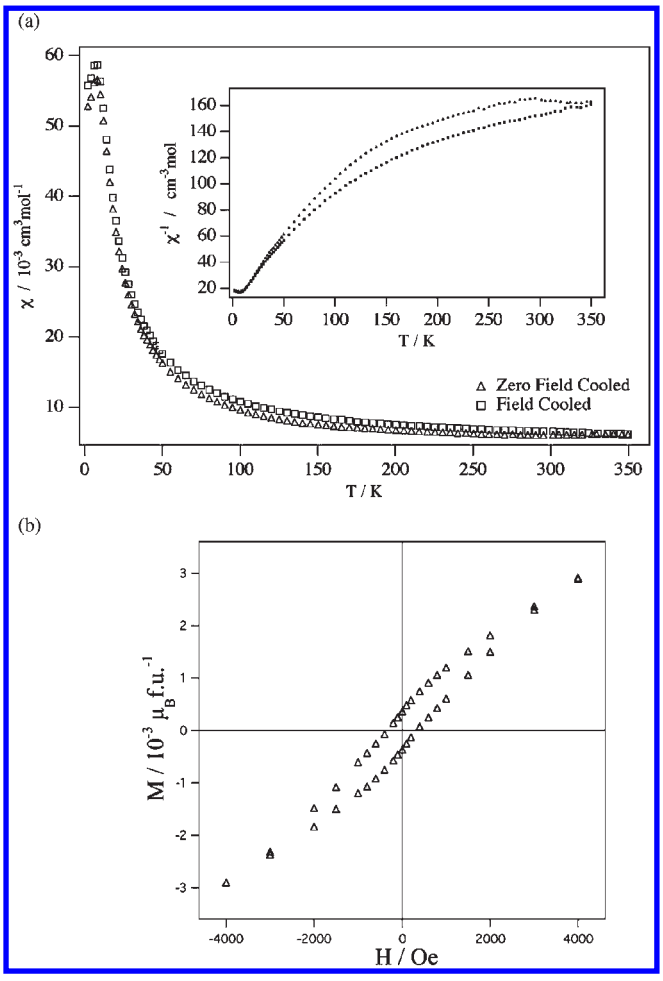

Figure 4. (a) Temperature dependence of the molar magnetic susceptibility of Co_2GeMo_3N and (b) field dependence of the magnetization of Co_2GeMo_3N at 300 K.

the sample contains a low concentration of a ferromagnetic impurity. No impurity was detected in our diffraction data, but the quantity of cobalt metal needed to produce the magnetization apparent in Figure 4b would be below the detection limit of our diffraction experiments.

In order to resolve the nature of the magnetic phase transition, Co_2GeMo_3N was studied by neutron diffraction. Data were collected at room temperature using a wavelength of ~1.59 Å and at 80 and 3.7 K using a wavelength of ~2.4 Å. In all cases, the data could be accounted for in terms of the nuclear scattering expected from an η-carbide structure with cobalt and germanium occupying the 32*e* and 16*d* sites, respectively. The results of the profile analysis of the data collected at room temperature are shown in Figure 5, and the refined structural parameters are listed in Table 1. The most important interatomic distances are listed in Table 2. Figure 6 shows a superposition of the low-angle portion of the diffraction patterns collected at 80 and 3.7 K; no additional Bragg peaks are observed on cooling the sample, nor do any of the peaks observed at room temperature show a significant increase in intensity. These data suggest that Co_2GeMo_3N does not show long-range magnetic order at 3.7 K, and that the susceptibility maximum at 8 K therefore does not signal a transition to a long-range ordered ground state.

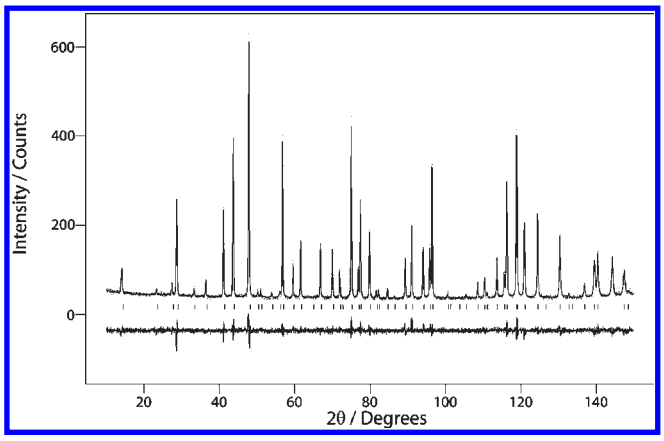

Figure 5. Observed, calculated, and difference neutron powder diffraction patterns of Co_2GeMo_3N at room temperature. Reflection positions are marked.

Table 1. Structural Parameters of Co_2GeMo_3N Derived from Neutron Diffraction Data[a]

		temperature/K		
		295	80	3.5
a/Å		11.0993(2)	11.0694(4)	11.0685(1)
R_{wp}, χ^2		8.0, 1.5	6.2, 2.4	6.2, 2.5
Co, 32*e*	*x*	0.2912(2)	0.2910(2)	0.2911(2)
	U_{iso}/Å^2	0.0057(8)	0.000(2)	0.005(2)
Ge, 16*d*	U_{iso}/Å^2	0.0088(4)	0.0023(7)	0.0032(7)
Mo, 48*f*	*y*	0.3179(1)	0.3181(1)	0.3179(1)
	U_{iso}/Å^2	0.0061(3)	0.0014(4)	0.0018(5)
N, 16*c*	U_{iso}/Å^2	0.0059(4)	0.0017(6)	0.0030(6)

[a] Space group $Fd\bar{3}m$; Co, 32*e* *x*, *x*, *x*; Ge 16*d* 0.5, 0.5, 0.5; Mo 48*f* *y*, 0.125, 0.125; N 16*c* 0, 0, 0.

Table 2. Interatomic Distances (Å) in Co_2GeMo_3N as a Function of Temperature

	temperature/K		
	295	80	3.5
Co−Co ×3	2.632(8)	2.629(7)	2.626(7)
Co−Ge ×3	2.406(2)	2.401(1)	2.400(1)
Co−Mo ×3	2.625(4)	2.616(3)	2.617(3)
Co−Mo ×3	2.806(1)	2.796(1)	2.798(1)
Ge−Mo ×6	2.8170(9)	2.808(1)	2.809(1)
Mo−Mo ×4	3.027(2)	3.022(2)	3.020(2)
Mo−Mo ×4	2.9160(6)	2.9074(6)	2.9077(7)
N−Mo ×6	2.1017(5)	2.0968(5)	2.0962(5)

However, we note that our data are of limited sensitivity; the Bragg scattering from an ordered moment of less than ~0.3 μ_B per 32*e* site would not be detectable above the background level.

ii. $Co_2Ge_{1-x}Ga_xMo_3N$. The observation of a magnetic phase transition, albeit ill-defined, at 8 K in Co_2GeMo_3N encouraged us to modify the composition in an attempt to raise the transition temperature. We were able to prepare monophasic (as judged by X-ray diffraction) samples of the η-carbide $Co_2Ge_{1-x}Ga_xMo_3N$ over the composition range $0 < x \leq 0.7$, a β-Mn impurity phase formed at higher concentrations of gallium. Unit cell parameters are listed in Table 3, and the temperature dependence of the resistivity for four pure samples is shown in Figure 7.

The temperature dependence of the magnetic susceptibility of selected compositions in the $Co_2Ge_{1-x}Ga_xMo_3N$

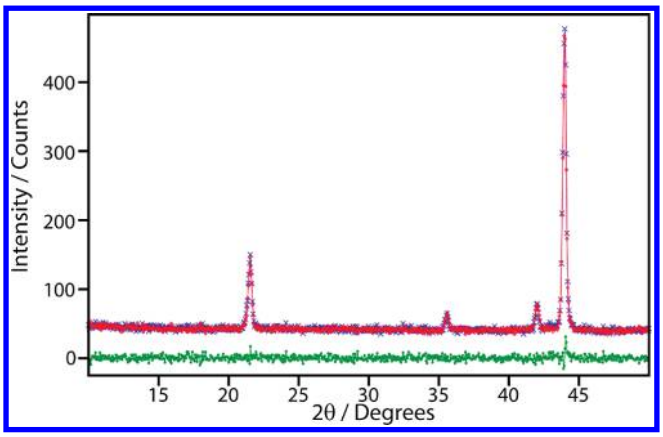

Figure 6. Low-angle region of the observed neutron diffraction patterns of Co_2GeMo_3N at 3.5 (blue ×) and 80 K (red ●). A difference curve is shown below.

Table 3. Unit-Cell and Magnetic Parameters of $Co_2Ge_{1-x}Ga_xMo_3N$

	x			
	0.1	0.3	0.5	0.7
a/Å	11.10484(9)	11.10899(9)	11.1100(1)	11.1194(1)
C/cm^3 K mol^{-1}	0.57(3)	0.76(3)	1.19(2)	2.6(1)
θ/K	16(5)	19(3)	−52(3)	−146(7)
α/cm^3 mol^{-1}	0.00155(8)	0.00094(7)	0.00017(5)	−0.0018(1)

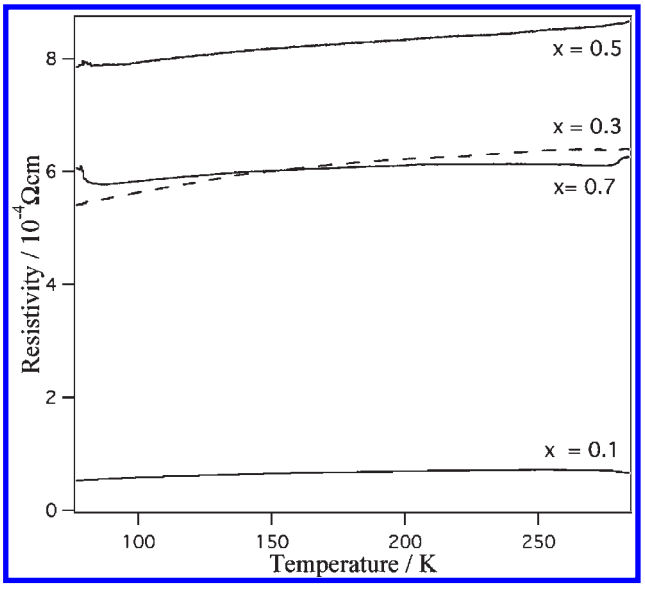

Figure 7. Temperature and composition dependence of the resistivity of $Co_2Ge_{1-x}Ga_xMo_3N$.

system is shown in Figure 8. In each case, both the ZFC and the FC susceptibilities show a maximum at a temperature that initially rises quickly as a function of gallium concentration before reaching a maximum value of 90 K when $x = 0.7$. No significant hysteresis is apparent between the ZFC and FC susceptibilities at 300 K for any composition, suggesting that these samples do not contain the ferromagnetic impurities that complicate the interpretation of the data presented in section i. Interestingly, hysteresis only becomes apparent in the susceptibilities of the compositions $x = 0.1$ and 0.3 below the temperature of the susceptibility maximum observed in the case of $x = 0.7$.

For each composition, attempts were made to fit $\chi(T)$ over the temperature range $150 < T/\mathrm{K} < 300$ to the equation $\chi = C/(T - \theta) + \alpha$, that is, to the Curie−Weiss law with an additional temperature-independent term. The temperature-independent term, α, models both the diamagnetism of the core electrons and any Pauli paramagnetic contribution from the conduction electrons. The resulting parameters are presented in Table 3.

The temperature dependence of the susceptibility of $Co_2Ge_{0.3}Ga_{0.7}Mo_3N$ indicated the existence of an antiferromagnetic state below 90 K, and a neutron diffraction study of this composition was therefore undertaken. A diffraction pattern collected at room temperature using a wavelength of 1.59 Å could be interpreted using a model based on the η-carbide structure with a disordered arrangement of germanium and gallium over the 16*d* sites. The refined structural parameters are listed in Table 4, and the most important interatomic distances are listed in Table 5. The observed and calculated diffraction profiles are shown in Figure 9. An increase in the intensity of some low-angle Bragg reflections, most notably 111, was apparent (Figure 10) when diffraction patterns collected at room temperature and 5 K using a wavelength of ∼2.4 Å were compared. This additional intensity could be accounted for if $Co_2Ge_{0.3}Ga_{0.7}Mo_3N$ was assumed to adopt the spin arrangement shown in Figure 11. The spins within each individual Co_4 tetrahedron are ferromagnetically aligned but the resultant moment of each tetrahedron is aligned antiparallel to those of the four nearest-neighbor tetrahedra. The magnetic structure can thus be said to consist of an antiferromagnetic arrangement of ferromagnetic Co_4 tetrahedra. The magnetic unit cell is the same size as the structural unit cell, and the face-centered symmetry is retained. However, the *d* glide plane is lost, and the configurational symmetry[20] belongs to the space group $F\bar{4}3m$, with the origin located at the center of a Co_4 tetrahedron. This model was able to account for the observed diffraction pattern, as can be seen in Figure 12, the ordered component of the magnetic moment on the 32*e* site refined to 0.48(9) μ_B. Note that the use of a polycrystalline sample limits the amount of information that can be deduced about the magnetic structure of a cubic material; we are not able to determine the direction along which the spins align. The structural parameters and bond lengths in the antiferromagnetic phase are included in Tables 4 and 5, respectively.

iii. $Co_{2-x}Fe_xGeMo_3N$. Having established that the temperature of the magnetic transition could be increased from the value of 8 K observed in Co_2GeMo_3N by the partial replacement of germanium by gallium, our next step was to attempt to induce an enhancement by the partial replacement of cobalt by iron. We were able to prepare polycrystalline η-carbide samples of both $Co_{0.5}Fe_{1.5}GeMo_3N$ and Fe_2GeMo_3N with unit cell parameters of 11.14886(8) and 11.15984(4) Å, respectively. The resistivity of Fe_2GeMo_3N was found to be 0.8×10^{-3} Ω cm at 300 K and almost constant over the temperature range $80 \leq T/\mathrm{K} \leq 300$. The resistivity of $Co_{0.5}Fe_{1.5}GeMo_3N$ was 1.6×10^{-3} Ω cm at 300 K and increased steadily to a value of 2.1×10^{-3} Ω cm on

(20) Shirane, G. *Acta Crystallogr.* **1959**, *12*, 282.

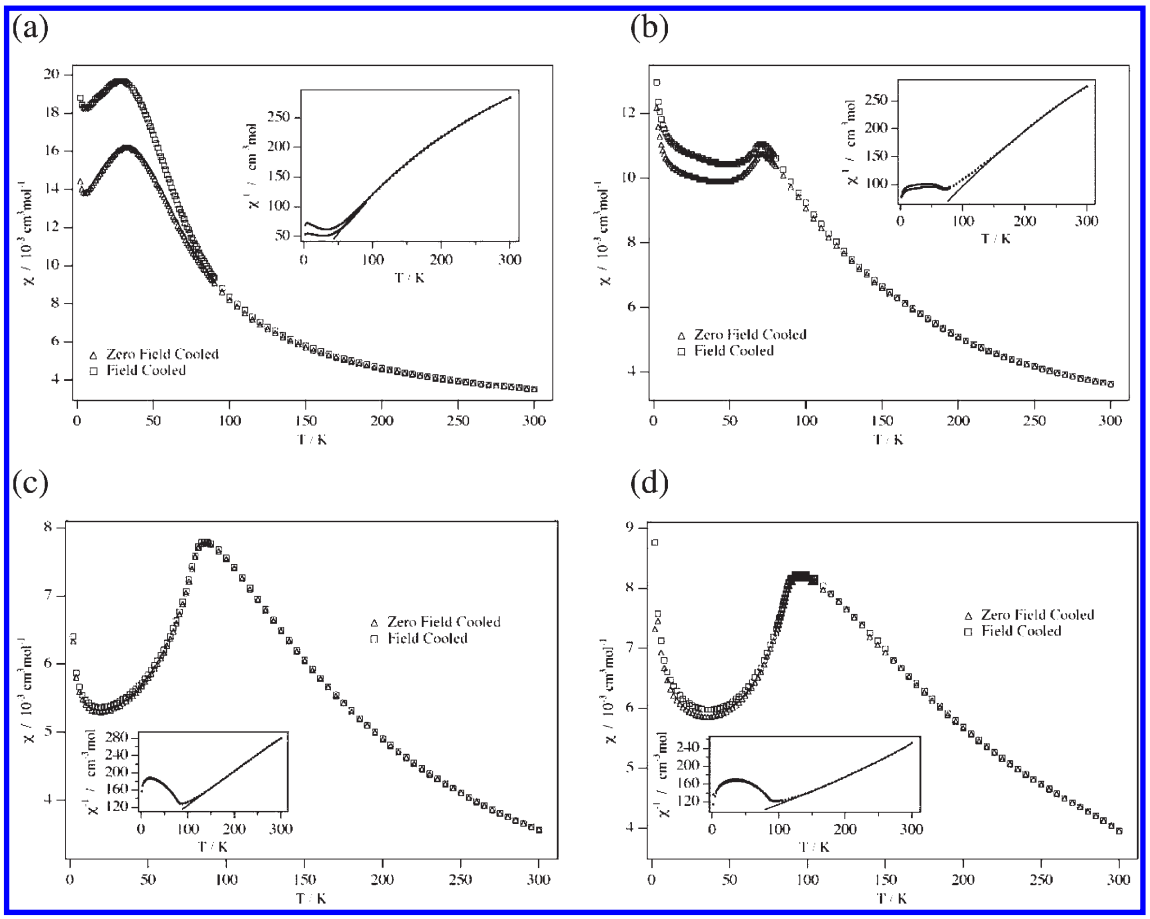

Figure 8. Temperature dependence of the molar magnetic susceptibility of $Co_2Ge_{1-x}Ga_xMo_3N$ for x = (a) 0.1, (b) 0.3, (c) 0.5, and (d) 0.7.

Table 4. Structural Parameters of $Co_2Ge_{0.3}Ga_{0.7}Mo_3N$ Derived from Neutron Diffraction Data[a]

		temperature/K	
		295	5
a/Å		11.1194(1)	11.1004(2)
R_{wp}, χ^2		7.8, 3.1	5.7, 2.0
Co, 32*e*	x	0.2909(2)	0.2903(3)
	U_{iso}/Å^2	−0.0006(7)	0.004(2)
Ge/Ga, 16*d*	U_{iso}/Å^2	0.0054(4)	0.0033(9)
Mo, 48*f*	y	0.3187(1)	0.3189(2)
	U_{iso}/Å^2	0.0029(2)	0.0020(6)
N, 16*c*	U_{iso}/Å^2	0.0026(3)	0.0033(8)

[a] Space group $Fd\bar{3}m$; Co, 32*e* x, x, x; Ge/Ga 16*d* 0.5, 0.5, 0.5; Mo 48*f* y, 0.125, 0.125; N 16*c* 0, 0, 0.

Table 5. Interatomic Distances (Å) in $Co_2Ge_{0.3}Ga_{0.7}Mo_3N$ as a Function of Temperature

	temperature/K	
	295	5
Co−Co ×3	2.643(6)	2.658(9)
Co−Ge/Ga ×3	2.412(1)	2.412(2)
Co−Mo ×3	2.628(3)	2.615(4)
Co−Mo ×3	2.802(1)	2.794(2)
Ge/Ga−Mo ×6	2.8156(9)	2.809(1)
Mo−Mo ×4	3.046(2)	3.044(3)
Mo−Mo ×4	2.9174(6)	2.9114(9)
N−Mo ×6	2.1089(5)	2.1062(7)

cooling to 80 K. The temperature dependence of the molar magnetic susceptibility of $Co_{0.5}Fe_{1.5}GeMo_3N$ is shown in Figure 13. A paramagnetic tail is apparent at the lowest temperatures, but the susceptibility is almost constant over the temperature range $50 < T/K < 200$. A gradual increase with increasing temperature is apparent above 250 K. This behavior was taken as evidence that $Co_{0.5}Fe_{1.5}GeMo_3N$ is in an antiferromagnetic state throughout the measured temperature range, with the hysteresis being attributable to a very low concentration of an impurity or to the glass-like freezing of some disordered spins. Neutron diffraction data were therefore collected at 295 K using a wavelength of 2.4 Å. The diffraction pattern could be interpreted in terms of an η-carbide phase with a disordered arrangement of cobalt and iron over the 32*e* sites and an ordered magnetic moment of 1.08(3) μ_B per site; the magnetic structure is the same as that of $Co_2Ge_{0.3}Ga_{0.7}Mo_3N$ described above and illustrated in Figure 11. The observed and calculated diffraction patterns are illustrated in Figure 14. The structural parameters and interatomic distances are listed in Tables 6 and 7, respectively.

Iron-57 Mössbauer spectra of $Co_{0.5}Fe_{1.5}GeMo_3N$ were measured at 10 and 295 K and are shown in Figure 15. The spectra confirm that this composition exhibits long-range magnetic order at 10 and 295 K. Our neutron diffraction study indicated that both the iron and cobalt, and only iron and cobalt, are found randomly distributed on the 32*e* site of $Co_{0.5}Fe_{1.5}GeMo_3N$. In its crystallographic structure, each 32*e* site has three 32*e* sites as

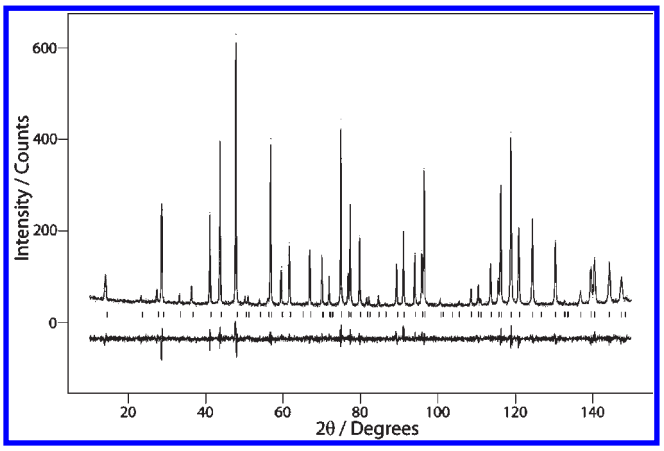

Figure 9. Observed, calculated, and difference neutron powder diffraction patterns of $Co_2Ge_{0.3}Ga_{0.7}Mo_3N$ at room temperature. Reflection positions are marked.

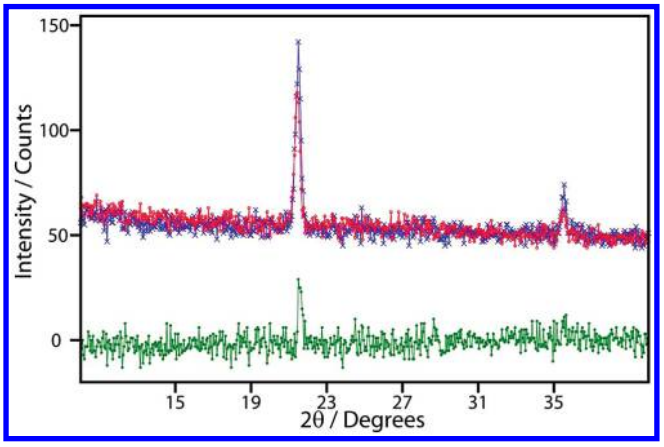

Figure 10. Low-angle region of the observed neutron diffraction patterns of $Co_2Ge_{0.3}Ga_{0.7}Mo_3N$ at 5 K (blue ×) and room temperature (red ●); a difference curve is shown below.

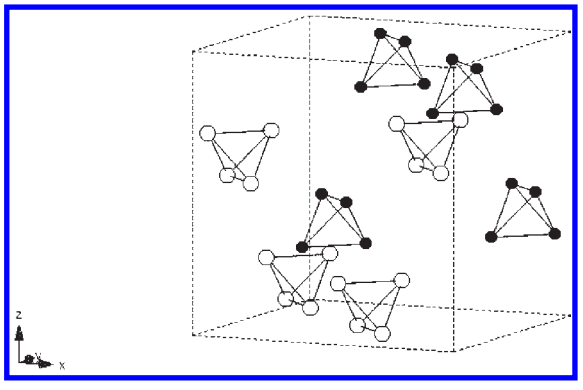

Figure 11. Magnetic structure of $Co_2Ge_{0.3}Ga_{0.7}Mo_3N$. Black and white circles represent Co atoms with opposite spin directions. Atoms less than 2.8 Å apart are joined by straight lines.

near-neighbors. As a consequence of the random binomial distribution of iron and cobalt on the 32*e* site, both the 10 and 295 K Mössbauer spectra of $Co_{0.5}Fe_{1.5}GeMo_3N$ exhibit a rather broad magnetic sextet. The magnetic spectra of $Co_{0.5}Fe_{1.5}GeMo_3N$ have been fit with four components whose relative areas have been obtained from a binomial calculation and constrained to 42.19% for three iron near neighbors, 42.19% for one cobalt and

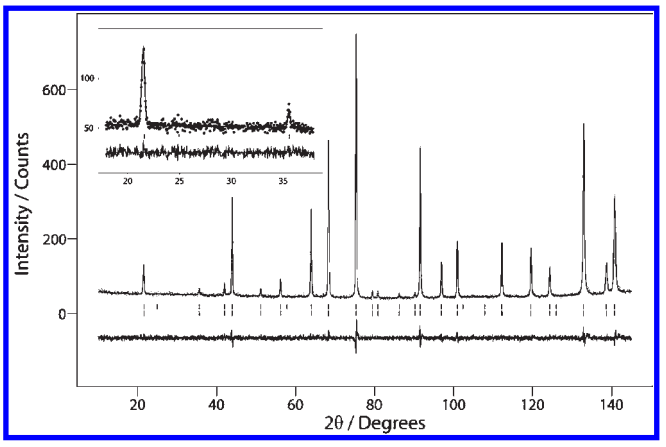

Figure 12. Observed, calculated, and difference neutron powder diffraction patterns of $Co_2Ge_{0.3}Ga_{0.7}Mo_3N$ at 5 K. The upper line of markers indicates the magnetic reflections.

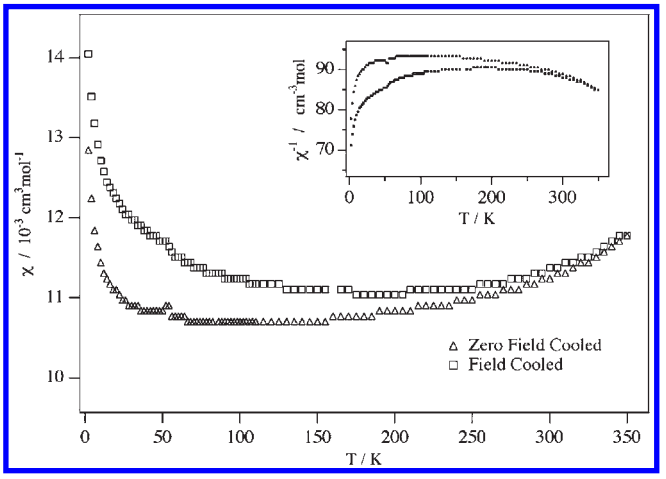

Figure 13. Temperature dependence of the molar magnetic susceptibility of $Co_{0.5}Fe_{1.5}GeMo_3N$.

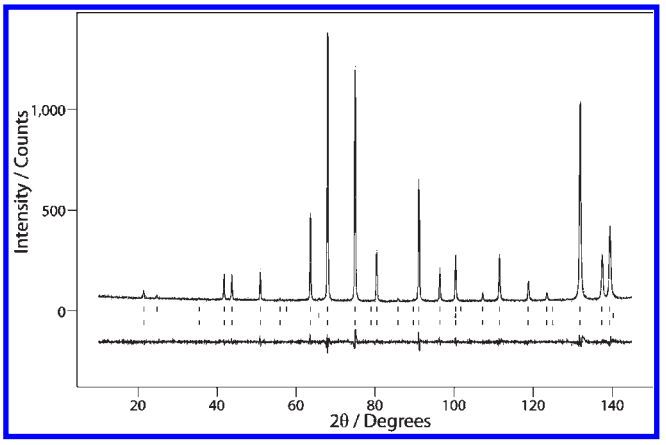

Figure 14. Observed, calculated, and difference neutron powder diffraction patterns of $Co_{0.5}Fe_{1.5}GeMo_3N$ at room temperature. Reflection positions are marked for, in descending order, the magnetic structure, the molybdenum impurity, and the crystal structure.

two iron near neighbors, 14.06% for two cobalt and one iron near neighbor, and 1.56% for three cobalt near neighbors. The results of these fits are shown as the four-component sextets in Figure 15, and the corresponding hyperfine parameters are given in Table 8. These fits were

Table 6. Structural Parameters of $Co_{0.5}Fe_{1.5}GeMo_3N$ at Room Temperature Derived from Neutron Diffraction[a]

a/Å		11.14886(8)
R_{wp}, χ^2		5.6, 2.6
Co/Fe, 32*e*	x	0.29202(9)
	U_{iso}/Å^2	0.0060(9)
Ge, 16*d*	U_{iso}/Å^2	0.0070(9)
Mo, 48*f*	y	0.3181(2)
	U_{iso}/Å^2	0.0054(5)
N, 16*c*	U_{iso}/Å^2	0.0066(7)

[a] Space group $Fd\bar{3}m$; Co/Fe, 32*e* x, x, x; Ge 16*d* 0.5, 0.5, 0.5; Mo 48*f* y, 0.125, 0.125; N 16*c* 0, 0, 0.

Table 7. Interatomic Distances (Å) in $Co_{0.5}Fe_{1.5}GeMo_3N$ at Room Temperature

Co/Fe−Co/Fe ×3	2.617(3)
Co/Fe−Ge ×3	2.4116(6)
Co/Fe−Mo ×3	2.649(1)
Co/Fe−Mo ×3	2.818(2)
Ge−Mo ×6	2.828(1)
Mo−Mo ×4	3.045(3)
Mo−Mo ×4	2.9280(8)
N−Mo ×6	2.1121(6)

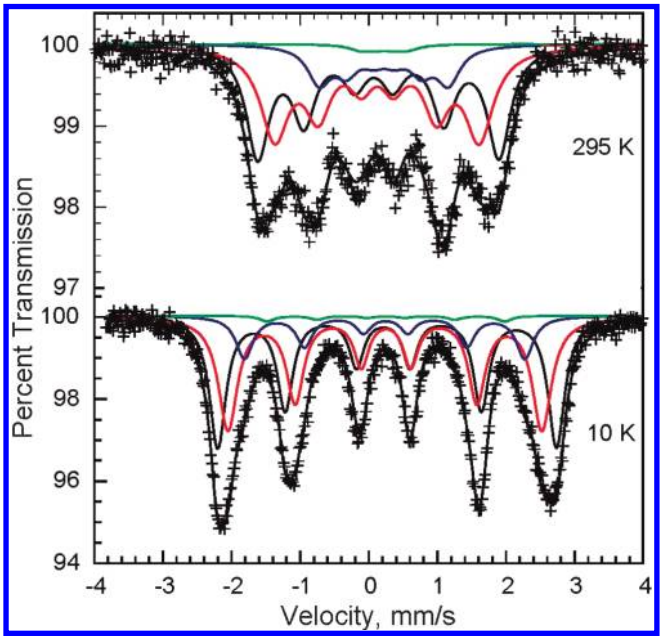

Figure 15. The Mössbauer spectra of $Co_{0.5}Fe_{1.5}GeMo_3N$ observed at 295 and 10 K.

constrained to have the same line width for each component sextet; no attempt was made to constrain the isomer shifts of the four components.

The assignment of the two sextets of equal relative areas given in Table 8 takes into consideration the observed[21,22] variation in the hyperfine field in iron−cobalt alloys as the number of cobalt near neighbors about an iron increases; that is, the hyperfine field increases as the percentage of cobalt increases from 0 to 33% and then decreases as the percentage of cobalt further increases. In a similar fashion, in $Co_{0.5}Fe_{1.5}GeMo_3N$, the iron nuclides with one cobalt and two iron near neighbors experience a

Table 8. Mössbauer Spectral Parameters[a] Obtained for $Co_{0.5}Fe_{1.5}GeMo_3N$

T, K	32*e* near neighbors	H, T	δ, mm/s[b]	QS, mm/s	Γ, mm/s	area, %
295	Fe_3	9.29(3)	0.112(3)	0.00	0.407(5)	42.19
	$CoFe_2$	10.92(2)	0.140(3)	0.059(5)	0.407(5)	42.19
	Co_2Fe	5.80(5)	0.21(1)	0.00	0.407(5)	14.06
	Co_3	1.9(4)	0.24	0.00	0.407(5)	1.56
10	Fe_3	14.21(2)	0.244(2)	−0.016(4)	0.251(5)	42.19
	$CoFe_2$	15.32(2)	0.238(2)	0.056(3)	0.251(5)	42.19
	Co_2Fe	12.68(4)	0.238(5)	−0.01(1)	0.251(5)	14.06
	Co_3	10.8(2)	0.24	0.00	0.251(5)	1.56

[a] The statistical errors are given. The lack of an error indicates that the parameter was constrained to the value given. [b] The isomer shifts are given relative to α-iron powder at 295 K.

larger hyperfine field than those with three iron near neighbors, and the iron nuclides with two or three cobalt near neighbors experience smaller hyperfine fields. At 295 K, the ratio of the weighted average hyperfine field of 9.37 T to the average 32*e* magnetic moment of 1.08 μ_B amounts to 8.68 T/μ_B, a value that is substantially smaller than the value of 15 T/μ_B commonly used in discussing iron intermetallic compounds. A comparison of the values measured in this work with those observed and calculated[23−25] in a series of ZFe_3N nitrides with the antiperovskite structure indicates that the small hyperfine fields observed herein and for the ZFe_3N nitrides result from the addition of two contributions, the core and valence contributions, with opposite sign. Hence, the ratios of the observed and calculated total hyperfine field to the iron magnetic moment are reduced from the usual value of 15 T/μ_B to a value between 6.15 and 12.7 T/μ_B.

Both magnetometry and Mössbauer spectral data indicated that Fe_2GeMo_3N also shows long-range magnetic order at room temperature. However, the behavior of this composition is clearly more complex than that of $Co_{0.5}Fe_{1.5}GeMo_3N$, and a full account will be presented at a later date.

iv. $Co_{2-x}Fe_xGe_{0.5}Ga_{0.5}Mo_3N$. The results described above demonstrate that the introduction of iron increases the strength of the magnetic interactions in these systems, as did the introduction of gallium into the $Co_2Ge_{1-x}Ga_xMo_3N$ system. We therefore investigated the system $Co_{2-x}Fe_xGe_{0.5}Ga_{0.5}Mo_3N$ in order to study the consequences of the cosubstitution of iron and gallium into Co_2GeMo_3N. The attempted syntheses of compositions $x = 0.5$, 0.6, 0.8, 1.5, and 2.0 all resulted in the formation of an η-carbide phase, but an additional β-manganese phase was always present at a low concentration (~3 wt %). The composition $x = 1.5$ also contained molybdenum metal, and $x = 2$ contained additional, unidentified impurities. A number of trial syntheses demonstrated that the β-manganese structure is not readily stabilized by germanium and iron; attempts to introduce the two elements into the structure simultaneously resulted in the formation of $FeMo_4Ge_3$, which was shown to be isostructural with Mo_5Ge_3.[26] Gallium can partner iron

(21) Johnson, C. E.; Ridout, M. S.; Cranshaw, T. E.; Madsen, P. E. *Phys. Rev. Lett.* **1961**, *6*, 450.
(22) Mancier, V.; Delplancke, J.-L.; Delwiche, J.; Hubin-Franskin, M.-J.; Piquer, C.; Rebbouth, L.; Grandjean, F. *J. Magn. Magn. Mater.* **2004**, *281*, 27.
(23) Mohn, P.; Schwarz, K.; Matar, S.; Demazeau, G. *Phys. Rev. B* **1992**, *45*, 4000.
(24) Paduani, C. *J. Magn. Magn. Mater.* **2004**, *278*, 231.
(25) Kuhnen, C. A.; de Figueiredo, R. S.; dos Santos, A. V. *J. Magn. Magn. Mater.* **2000**, *219*, 58.
(26) Baker, P. J.; Battle, P. D.; Blundell, S. J.; Grandjean, F.; Lancaster, T.; Long, G. J.; Oldham, S. E.; Prior, T. J. *Phys . Rev. B* **2008**, *77*, 134405.

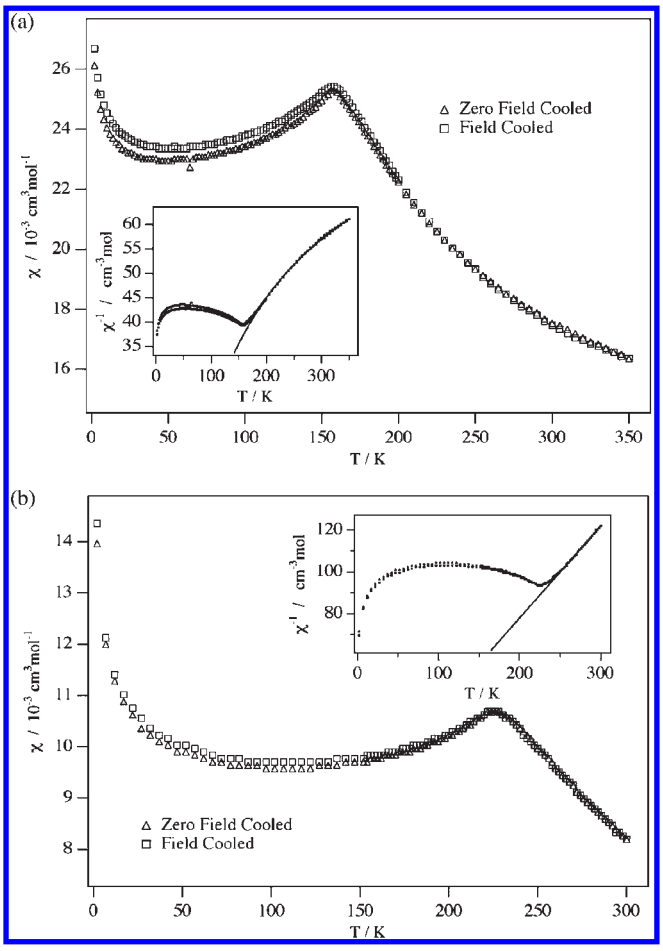

Figure 16. Temperature dependence of the molar magnetic susceptibility of (a) $Co_{1.5}Fe_{0.5}Ge_{0.5}Ga_{0.5}Mo_3N$ and (b) $Co_{1.2}Fe_{0.8}Ge_{0.5}Ga_{0.5}Mo_3N$.

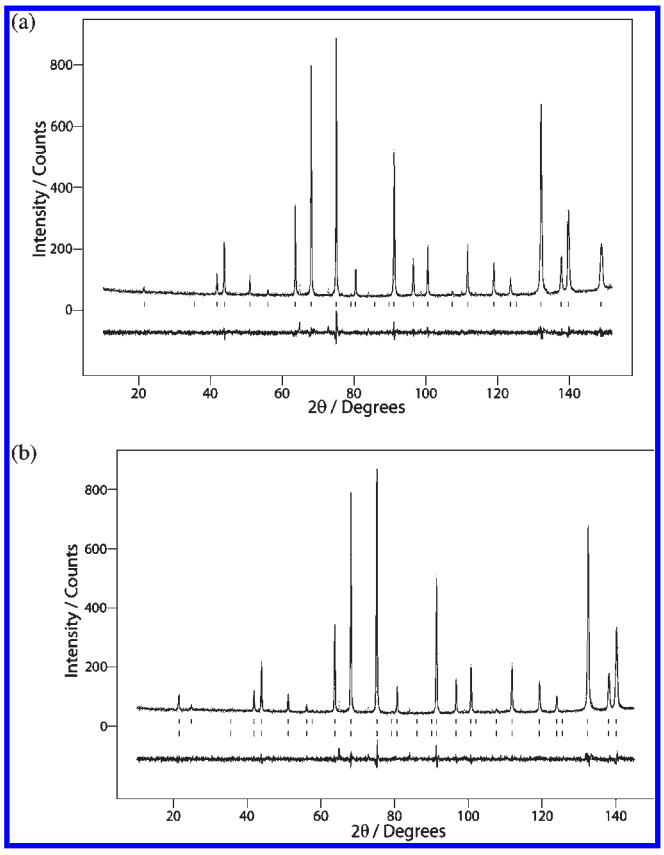

Figure 17. Observed, calculated, and difference neutron powder diffraction patterns of $Co_{1.2}Fe_{0.8}Ge_{0.5}Ga_{0.5}Mo_3N$ at (a) room temperature and (b) 10 K. The upper line of markers indicates the magnetic reflections. Unmarked reflections ($2\theta \sim 64$, 73, and 84°) derive from a second phase with a β-Mn structure.

in the β-manganese structure, although $Fe_{1.25}Ga_{0.75}Mo_3N$ was the only composition that could be prepared in the system $Fe_{2-x}Ga_xMo_3N$. The $Co_{2-x}Ga_xMo_3N$ system has been less thoroughly studied, but we have prepared a monophasic sample of composition $Co_{1.04}Ga_{0.96}Mo_3N$. No Néel or Curie point was seen in the magnetic susceptibility of either of these β-manganese phases. On the basis of these data, we assumed that the β-manganese impurity phase in $Co_{2-x}Fe_xGe_{0.5}Ga_{0.5}Mo_3N$ ($x \leq 0.8$) probably contained iron, cobalt, and gallium in an unknown ratio and, more importantly, that it did not order magnetically above 5 K; any magnetic transition in the susceptibility of the impure reaction product can then be attributed to the η-carbide phase. With this assumption, we proceeded to characterize more fully $Co_{2-x}Fe_xGe_{0.5}Ga_{0.5}Mo_3N$ for $x = 0.5$ and 0.8; the unit-cell parameters of the η-carbide phases in these two samples refined to 11.12799(5) and 11.13765(5) Å. The temperature dependence of the molar magnetic susceptibility of each composition is shown in Figure 16, together with a fit to a Curie−Weiss law with a constant term added. The susceptibility shows a maximum at 156 and 228 K for $x = 0.5$ and 0.8, respectively. As a consequence of the relatively high transition temperatures, the data above the transitions could only be fitted over a limited temperature range, particularly in the case of $x = 0.8$. This, together with the presence of an impurity, raises doubts about the validity of the fitted parameters which were, for $x = 0.5$ and 0.8, respectively $C = 1.80(6)$ and 2.3(2) cm^3 K mol^{-1}, $\theta = 49(4)$ and 21(9) K, and $\alpha = 0.0104(1)$ and $-0.001(3)$ cm^3 mol^{-1}. The positive Weiss temperatures are clearly incompatible with the antiferromagnetic ordering suggested by the susceptibility maximum. $Co_{1.2}Fe_{0.8}Ge_{0.5}Ga_{0.5}Mo_3N$ was studied by neutron powder diffraction at 5 and 295 K; a wavelength of 2.4 Å was used in both experiments. The data collected at ambient temperature contained strong peaks from an η-carbide phase and weak peaks from a β-manganese phase. The structure of the former was refined using the target stoichiometry, although it is likely to be slightly germanium-rich. The structure of the latter was not refined because of the relatively large uncertainty in the composition. The observed and calculated diffraction patterns are shown in Figure 17a; the most obvious positive features in the difference curve ($2\theta \sim 64$, 73, and 84°) correspond to the unfitted Bragg peaks of the β-manganese phase. Additional Bragg scattering was apparent in the data collected at 10 K. This could be accounted for by assuming that the η-carbide phase adopts the magnetic structure shown in Figure 11 at low temperatures; the ordered component of the magnetic moment then refined to 1.17(4) μ_B per 32*e* site. The low-temperature diffraction profiles are shown in Figure 17b, and the coordinates and interatomic distances at both room temperature and 10 K are listed in Tables 9 and 10, respectively.

Table 9. Structural Parameters of $Co_{1.2}Fe_{0.8}Ge_{0.5}Ga_{0.5}Mo_3N$ Derived from Neutron Diffraction[a]

		temperature/K	
		295	5
a/Å		11.13765(5)	11.1264(3)
R_{wp}, χ^2		5.3, 2.5	5.5, 2.6
Co/Fe, 32*e*	x	0.2918(1)	0.2919(2)
	U_{iso}/Å^2	0.010(1)	0.008(1)
Ge/Ga, 16*d*	U_{iso}/Å^2	0.0072(9)	0.004(1)
Mo, 48*f*	y	0.3184(2)	0.3182(2)
	U_{iso}/Å^2	0.0065(6)	0.0030(6)
N, 16*c*	U_{iso}/Å^2	0.0080(8)	0.0044(9)

[a] Space group $Fd\bar{3}m$; Co/Fe, 32*e* *x*, *x*, *x*; Ge/Ga 16*d* 0.5, 0.5, 0.5; Mo 48*f* *y*, 0.125, 0.125; N 16*c* 0, 0, 0.

Table 10. Interatomic Distances (Å) in $Co_{1.2}Fe_{0.8}Ge_{0.5}Ga_{0.5}Mo_3N$ as a Function of Temperature

	295 K	5 K
Co/Fe−Co/Fe ×3	2.622(5)	2.616(5)
Co/Fe−Ge/Ga ×3	2.4107(9)	2.408(1)
Co/Fe−Mo ×3	2.644(2)	2.642(2)
Co/Fe−Mo ×3	2.813(2)	2.812(2)
Ge/Ga−Mo ×6	2.823(1)	2.821(2)
Mo−Mo ×4	3.046(3)	3.040(3)
Mo−Mo ×4	2.9238(8)	2.9217(9)
N−Mo ×6	2.1110(7)	2.1082(7)

Discussion

The results described above demonstrate the chemical flexibility of the η-carbide structure with respect to nitride formation. Germanium is readily accommodated on the 16*d* site, and some substitution by gallium can be tolerated. However, the presence of gallium makes the formation of a β-manganese phase more competitive, and the composition range over which pure η-carbide materials could be prepared was limited in mixed Ge/Ga systems. We shall return to this point below. The unit cell parameters of those compositions containing a p-block element were systematically larger than those of compositions containing only d-block elements, for example, $Fe_{3-x}Co_xMo_3N$.[17] This can be attributed to the occupation of states derived from the 4s and 4p atomic orbitals of the p-block element, and as a consequence the distance between neighboring 32*e* sites is increased by ~4%. The distance between the 32*e* site and the 16*d* site also increases, but by only ~1.5%. The mean distance between the 32*e* site and the 48*f* (Mo) site increases, but not in a uniform manner. The increased unit-cell parameter has little consequence for the mean Mo−Mo distance, although the difference between the two distinct values that contribute to the mean is always smaller in the presence of germanium or gallium. The Mo−N distance is essentially independent of the composition. The most significant structural changes thus occur around the site occupied by the magnetic atoms, an observation that is consistent with the marked changes in magnetic behavior that our strategy has produced.

The resistivity of all compositions in the series $Ni_{2-x}Co_xGeMo_3N$ shows a positive temperature coefficient and a magnitude of $\sim 10^{-3}$ Ω cm. This justifies their being described as "bad metals". In view of the dependence of the measured resistivity on the sample preparation, it is impossible to identify with confidence a clear trend with the composition. The magnetic susceptibility of compositions in this series shows a marked increase on cooling below 50 K, although the effect is on a much smaller scale than that observed previously in $Fe_{3-x}Co_xMo_3N$;[17] the magnitude of the susceptibility at 2 K increases with increasing cobalt concentration. One possible explanation for this is that, with increasing concentration, nearest-neighbor cobalt atoms couple to each other ferromagnetically to form superparamagnetic tetrahedra, which, unlike in the $Fe_{3-x}Co_xMo_3N$ solid solution, are isolated from each other by diamagnetic atoms on the 16*d* sites. It is then the resultant magnetic moments of the tetrahedra that are aligned by the applied field at low temperatures. The extreme case, in which tetrahedra of d-block metals are truly isolated, has been considered in detail for iron, with the conclusion that ferromagnetic Fe_4 tetrahedra are relatively stable.[27] The magnetic transition seen at 8 K in Co_2GeMo_3N can then be ascribed to a spin-glass-like freezing of the magnetic moments on the isolated Co_4 tetrahedra.

The introduction of gallium into the system increases the unit-cell parameter and decreases the number of electrons in the orbitals having 4p parentage. Extensive band-structure calculations on these disordered systems will be necessary in order to understand how the additional hole in the p levels modifies the electronic structure, but it is clear that the strength of the magnetic coupling between cobalt atoms in different tetrahedra increases and our neutron diffraction data prove the existence of a long-range ordered ground state in $Co_2Ge_{0.3}Ga_{0.7}Mo_3N$, albeit with a very low ordered magnetic moment on each 32*e* site. The parameters derived from fitting $\chi(T)$ in the high-temperature region illustrate the change in magnetic behavior with the composition. The Weiss temperature, θ, is positive for $x = 0.1$ and 0.3, but negative for $x = 0.5$ and 0.7. This decrease indicates that ferromagnetic interactions dominate at low gallium concentrations but that antiferromagnetic coupling dominates at higher concentrations. The increase in the Curie constant, C, and the decrease in α suggest that the number of unpaired electrons increases as gallium is added. However, the mean ordered moment at the 32*e* site in $Co_2Ge_{0.3}Ga_{0.7}Mo_3N$ is much lower than would be expected on the basis of the Curie constant. This suggests that there is some residual spin frustration, which might be responsible for the low-level hysteresis seen in the susceptibility of $x = 0.7$ below the Néel temperature. The absence of hysteresis at temperatures higher than that of the maximum in the susceptibility of $Co_2Ge_{0.5}Ga_{0.5}Mo_3N$ suggests that this composition might also show long-range magnetic order. The susceptibilities of $Co_2Ge_{1-x}Ga_xMo_3N$ with $x = 0.1$ and 0.3 show hysteresis below the Néel temperature of $x = 0.7$, perhaps indicating that the interatomic exchange interactions that cause long-range magnetic order in $Co_2Ge_{0.3}Ga_{0.7}Mo_3N$ are not negligible in the germanium-rich compositions, but neither are they strong enough to induce long-range order. Muon spin relaxation studies might be able to clarify these issues in the future.

The proposed magnetic structure and the variation of the Curie−Weiss parameters with composition are both consistent with the hypothesis that ferromagnetic Co_4 tetrahedra play a central role in the magnetism of these compounds; the structure drawn in Figure 11 consists of an antiferromagnetic

(27) Chen, J. L.; Wang, C. S.; Jackson, K. A.; Pederson, M. R. *Phys . Rev. B* **1991**, *44*, 6558.

arrangement of these ferromagnetic tetrahedra. A comparison of Figures 1a and 11 reveals that the resultant moment of each tetrahedron is aligned antiparallel with respect to those of the four tetrahedra to which it is linked by face-capping p-block atoms. We propose that the changes in the electronic structure brought about by the introduction of gallium cause the ferromagnetic Co_4 clusters to couple together in an antiferromagnetic manner and that this coupling is strong enough to create an antiferromagnetic ground state when $x = 0.7$.

Band-structure calculations should also be able to elucidate the parentage of the orbitals which contribute to the Fermi surface and, hence, account for the coexistence of magnetic order and the metallic conductivity apparent in Figure 7. These transport data, like those in Figure 2, show a low metallic conductivity, but the limited accuracy of our experiment again precludes detailed interpretation of the composition dependence. The local minimum in the resistivity of $Co_2Ge_{0.3}Ga_{0.7}Mo_3N$ at a temperature close to the Néel point is likely to reflect the onset of domain-wall scattering. Our transport data do not extend to low enough temperatures to reveal similar features in the behavior of other compositions. We do not presently have an explanation for the increase in the resisitivity of the same composition at ~275 K, but both of these features were reproduced in data collected on a second sample.

The introduction of iron into Co_2GeMo_3N produces a more dramatic effect than the introduction of gallium. The atom pairs (Co, Ga) and (Fe, Ge) are isoelectronic, but as a result of the relative multiplicities of the 16*d* and 32*e* sites, together with the apparent preference of gallium for the β-manganese structure, the substitution of iron for cobalt allows a wider range of electron concentrations to be sampled than does that of gallium for germanium. The reduction in the total electron count results in an increase in the Néel temperature to an as-yet undetermined value above 350 K for $Co_{0.5}Fe_{1.5}GeMo_3N$; a similar increase occurs in the more complex case of Fe_2GeMo_3N. The mean ordered magnetic moment on the 32*e* site of $Co_{0.5}Fe_{1.5}GeMo_3N$ is larger at 295 K than that measured for $Co_2Ge_{0.3}Ga_{0.7}Mo_3N$ at 5 K, and the Mössbauer spectral data in Table 8 show that the moment on the iron sites of $Co_{0.5}Fe_{1.5}GeMo_3N$ increases by ~50% on cooling to 10 K. $Co_{0.5}Fe_{1.5}GeMo_3N$ is the only sample studied in this work to show a negative temperature coefficient of resistivity. The significance of this difference is not yet clear.

The cosubstitution of cobalt by iron and germanium by gallium also leads to an enhancement of the Néel temperature. The electron count of $Co_{0.7}Fe_{1.3}GeMo_3N$ would be equal to that of $Co_{1.2}Fe_{0.8}Ge_{0.5}Ga_{0.5}Mo_3N$, and that of $CoFeGeMo_3N$ to that of $Co_{1.5}Fe_{0.5}Ge_{0.5}Ga_{0.5}Mo_3N$. The antiferromagnetic ordering temperature thus increases as the electron count in these systems decreases. The behavior of $Co_2Ge_{0.3}Ga_{0.7}Mo_3N$, which has has a higher electron count than any of the iron-containing systems, is consistent with this observation. It is thus possible to develop a model to correlate the Néel temperature with the total electron count, and then to hypothesize that Fe_3Mo_3N and the solid solution $Fe_{3-x}Co_xMo_3N$ are too electron-rich to show long-range order. This simplistic model ignores the fact that, in $Fe_{3-x}Co_xMo_3N$, the highest occupied orbitals associated with the 16*d* site will derive largely from atomic 3d orbitals, whereas in the gallium and germanium compounds, they will derive from 4s and 4p orbitals, which are likely to give rise to a larger bandwidth. Co_2GeMo_3N, with a total of 22 valence electrons on the atoms occupying the 16*d* and 32*e* sites, perhaps provides a better definition of a nonmagnetic electron-rich composition in this context. Band-structure calculations should be able to clarify the situation, and it is certainly possible to test the model by synthesizing further compositions in the solid solutions discussed above. It should also be noted that the ordering temperature increases as the unit-cell parameter increases. In a metallic system wherein the RKKY interaction is likely to dominate the exchange interactions, the strength of the interatomic coupling will be sensitive to the interatomic distance. However, the interatomic distance will be partly determined by the number of occupied states in the conduction band, that is, whether the electrons at the Fermi level are occupying bonding or antibonding states. The introduction of too much gallium leads to a paucity of electrons, hence weaker bonding and instability with respect to the β-manganese structure.

To conclude, our strategy of introducing a p-block element onto the 16*d* site of the η-carbide structure has enabled us to prepare a number of new, magnetically ordered phases. Their electronic properties are clearly sensitive to the total electron count and to the parentage of the orbitals near the Fermi energy. However, a number of issues concerning these materials remain unresolved. Further experimental and theoretical studies which address them are underway.

Acknowledgment. One of us (LAS) is grateful to the Rhodes Trust for the provision of a postgraduate scholarship. The authors thank Dr. M. T. Sougrati for his help in obtaining the Mössbauer spectra and Dr. E. Suard for assistance at ILL Grenoble. F.G. acknowledges the financial support of the Fonds National de la Recherche Scientifique, grants 9.456595 and 1.5.064.05.